DOI: 10.15480/882.9363

Eighth International Symposium on Marine Propulsors
smp'24, Berlin, Germany, March 2024

Study of Rudder Drag in Propeller Slipstream Using Segmented Model Rudder

Takashi Kanemaru[1], Akira Yoshitake[1], Jun Ando[1]

[1]Faculty of Engineering, Kyushu University, Fukuoka, Japan

ABSTRACT

It is very important to estimate the interaction between propeller and rudder because a rudder in the propeller slipstream generates thrust. It is possible to predict the energy-saving effect by numerical methods such as theoretical calculation based on potential flow theory or CFD, qualitatively. However, the partial rudder drag just behind the boss cap is difficult to simulate since the interaction between a hub vortex and the rudder surface is very complicated. In the case of potential flow theory, the partial force on the center of the rudder can be either drag or thrust, depending on how the hub vortex is treated.

This paper focuses on the partial rudder drag in order to clear not only the total rudder drag but also how the hub vortex interacts with the rudder. Knowing these phenomena is very important to check the validity of numerical methods. The authors conducted an experiment on the interaction between propeller and rudder using the segmented model rudder. The rudder is divided into three parts, upper, center, and lower part. The experimental results show that the rudder thrust is largest at the center part. Also, the experimental results are compared to the calculated results in order to validate both of them.

Keywords

Propeller-rudder interaction, Segmented model rudder, Rudder drag in slipstream, Rudder drag distribution, SQCM

1 INTRODUCTION

Recently the development and improvement of energy-saving devices have been conducted actively to reduce CO2 emissions. If we focus on the propulsive performance, the rudder can be regarded as one of the energy-saving devices that recover the energy from the circumferential flow produced by the working propeller, which does not contribute to the propulsion. This effect is obtained as rudder thrust that is generated in the propeller slipstream. The characteristics of the propulsive performance can be simulated by panel method and CFD to some extent. On the other hand, the phenomenon is very complicated around the rudder surface where the hub vortex generated by a working propeller goes through. We think that the partial rudder force here is very important to calculate the rudder drag because the circumferential flow is very large around here. However, the calculation is very difficult and this is a reason why the quantitative estimation of the rudder thrust in the slipstream is difficult. In order to predict the rudder drag accurately, the rudder drag distribution in the spanwise direction should be shown. But it is very difficult experimentally. The pressure measurement on a rudder surface in a slipstream like Moriyama's experiment (1981) can be a method to know the uncertain force like the partial force at the center of the rudder. However, his experiment doesn't have enough data which show the details of the force.

The authors developed a panel method that can take the hub vortex into consideration and applied it to the interaction problem between propeller and rudder. In the case of panel method, the partial rudder force just behind the propeller boss cap can be either drag or thrust depending on the modeling of the hub vortex. Also, in the case of CFD, very fine mesh is required in the slipstream, especially around the hub vortex. If this is not satisfied, the calculated results are not always reliable.

In this study, as a method to generally understand the rudder drag distribution, we divide the model rudder in slipstream into three parts, upper, center, and lower, and try to experimentally obtain each force. In particular, we investigate the rudder force at the center part. Furthermore, we validate the experimental data by comparing both the experimental data and the calculated panel method results.

2 RUDDER DRAG IN PROPELLER SLIPSTREAM

The rudder force F_X in propeller slipstream consists of three components which are the drag by the viscosity F_D, the drag by the pressure gradient F_P and the rudder thrust F_T. The latter two components are the characteristic forces due to the propeller-rudder interaction.

$$F_X = F_D + F_P + F_T \quad (1)$$

The propeller slipstream has the velocity gradient in the axial direction by the accelerated flow produced by the working propeller. Therefore, the pressure field behind the propeller has a negative gradient according to the positive gradient of the axial velocity in the propeller slipstream. As

the result, the drag acts on the rudder in the propeller slipstream because the pressure field on the trailing edge side is lower than that on the leading edge side (Figure 1). This is the mechanism of the drag by the pressure gradient F_P.

On the other hand, the rudder behind the propeller generates the thrust owing to the circumferential flow in the propeller slipstream. The inflow velocity vector at the rudder section has the attack angle as the composed velocity vector from the axial and circumferential flow components and the forward component of the lift produced by the inflow with the attack angle becomes the thrust (Figure 1). The rudder thrust $F_T(< 0)$ reduces the rudder drag F_X and contributes to the propulsive performance.

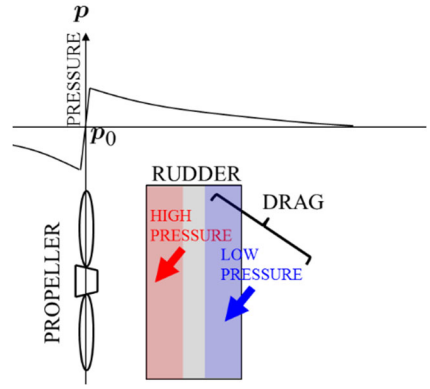

Drag by pressure gradient

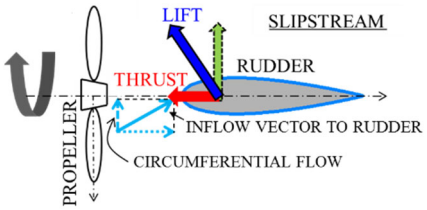

Rudder thrust

Figure 1 Rudder forces in propeller slipstream

3 EXPERIMENT

3.1 Original rudder and propeller

We select the rudder MR-2 as the model rudder (Table 1), which has much informative data regarding the propeller-rudder interaction in the study by Moriyama (1981).

Table 1 Principal particulars of rudder

NAME OF RUDDER	ORIGINAL (MR-2)
CHORD LENGTH (m)	0.200
SPAN LENGTH (m)	0.300
ASPECT RATIO	1.50
TYPE OF SECTION	NACA0015

Also we adopt the model propeller MP-B (Table 2) which was used in the propeller-rudder interaction study by Moriyama & Yamazaki (1981).

Table 2 Principal particulars of propeller

NAME OF PROPELLER	MP-B
DIAMETER (m)	0.2389
NUMBER OF BLADE	5
PITCH RATIO AT 0.7R	0.679
EXPANDED AREA RATIO	0.610
HUB RATIO	0.179
RAKE ANGLE (DEG.)	9.17
BLADE SECTION	AU

Figure 2 Model propeller MP-B

3.2 Divided Model Rudder

In this experiment, the rudder shown in Table 1 is divided into three parts. Two types of cases are adopted for how to divide as shown in Figure 3. In Case 1, the center (red) edge corresponds to 0.5R of the propeller (R is the propeller radius). In Case 2, it corresponds to the propeller hub diameter. Figure 4 shows these models.

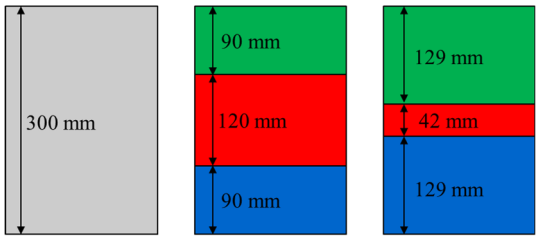

Figure 3 Segmented patterns

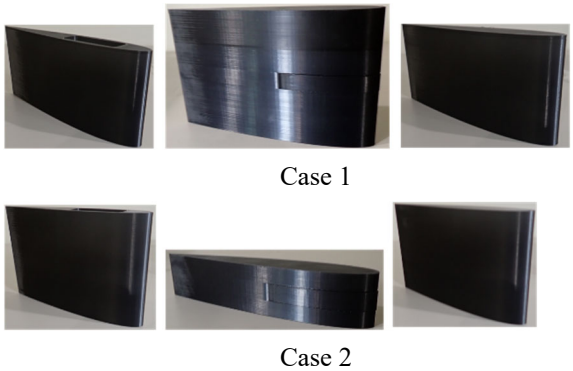

Figure 4 Segmented model rudders

3.3 Measurement

The measurements of the rudder force in the propeller-rudder interaction were conducted in high speed circulating water channel of Kyushu University (Figure 5) The drag of the rudder shaft can be removed by the shaft cover which has the same wing section as the rudder. Also, the free surface cover makes it possible to measure the rudder drag without the wave resistance caused by the open water propeller test boat.

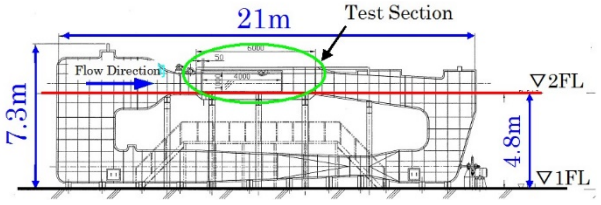

Figure 5 High speed circulating water channel

Due to the experimental equipment, the rudder drag can only be measured at the upper part. A platform is installed in the test section to fix the lower part of the rudder and measurements are conducted changing the dividing positions (the lower end of the lower part, the lower end of the center part, and the upper end of the center part). The force of each part is calculated by subtracting the partial forces which have different dividing positions. Details are shown in the next section. Figure 6 shows a schematic diagram of the experiment. Figure 7 shows an experiment condition of Case 2 in which the upper and middle parts are merged, and the middle part and the lower part are separated. The gap of dividing is set to 0.5 mm which is the minimum not to contact to the next part.

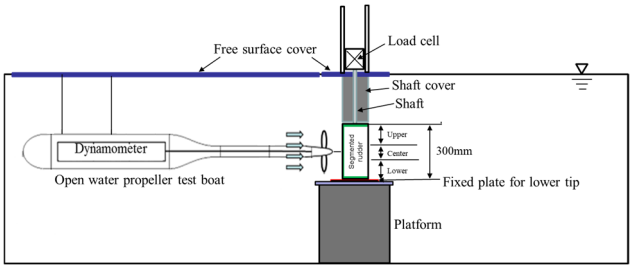

Figure 6 Test section in operating condition

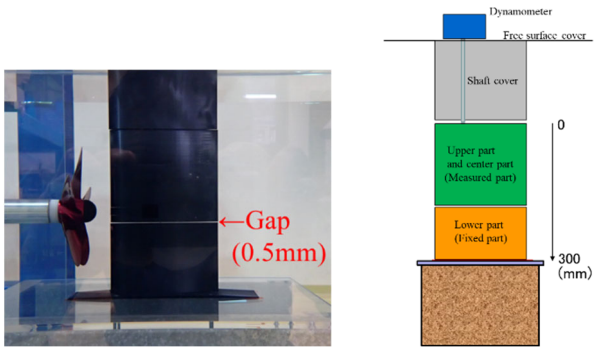

Figure 7 Experimental condition of Case 2

3.4 Method to extract part force

The force of each part can be calculated using the results of the five pattern measurements (Figure 8). Figure 9 shows how to calculate the force of the lower part. First, the total force of the upper, center, and lower parts is measured using all combined model rudders. Here, the bottom of the model is not fixed and given a gap. Next, the rudder force combining the upper and the center parts is measured with the fixed lower part of the platform. The force of the lower part is calculated by subtracting the force of the upper and center from the total force.

Figure 10 shows how to calculate the force of the center part. The rudder force of the center part can be calculated by subtracting the force of the upper part from that of the combined upper and center parts.

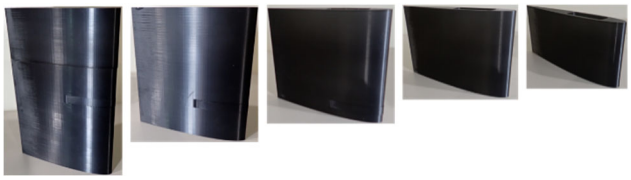

Figure 8 Model rudders of measurement part

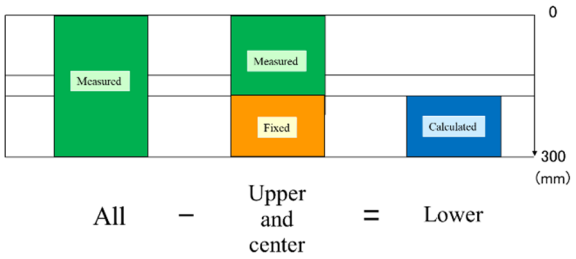

Figure 9 Drag calculation of lower part

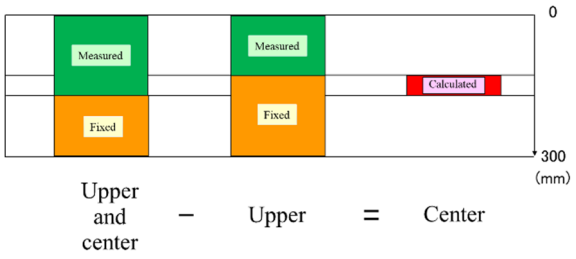

Figure 10 Drag calculation of center part

4 CALCULATION

The calculation method for the propeller-rudder interaction problem is based on a simple surface panel method "SQCM" (Nakatake et al. 1994, Ando et al. 1995, Maita et al. 1997). SQCM (Source and QCM) uses source distributions (Hess & Smith 1964) on the propeller blade surface and the rudder surface. Also, discrete vortex distributions are arranged on their mean camber surfaces according to QCM (**Q**uasi-**C**ontinuous vortex lattice **M**ethod) (Lan 1974). These singularities should satisfy the

boundary condition that the normal velocity is zero on the propeller blade surface, the rudder surface, and their mean camber surfaces. In order to consider the effect of the hub vortex, the hub vortex model (Figure 11 (Kanemaru et al. 2013)) for SQCM is incorporated into this calculation method in which the lifting surfaces of each blade are extended to the inside of the hub and the propeller shaft center line is regarded as the hub vortex line. This hub vortex model is also useful for energy-saving devices performance prediction. (e.g., Ryu et al. 2014).

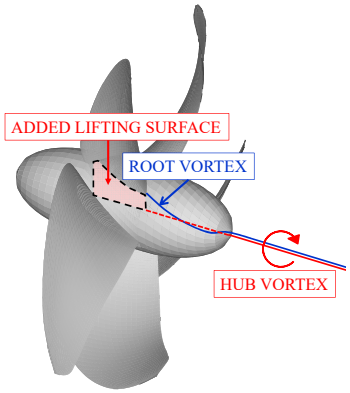

Figure 11 Outline of hub vortex model

The propeller coordinate system $o-xyz$ and the rudder coordinate system $o_r-x_ry_rz_r$ which is shifted from $o-xyz$ with the distance ℓ on the x -axis are introduced as Figure 12. The z_r-axis passes through the leading edge line of the rudder.

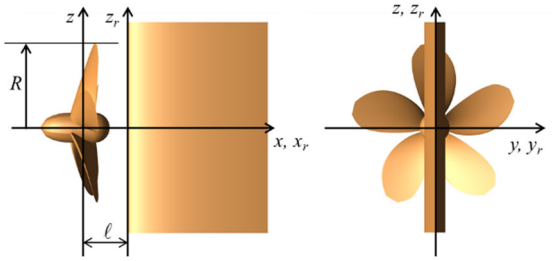

Figure 12 Coordinate systems of propeller and rudder

It is very difficult to calculate the singularity distribution on the rudder because of the singularity problem caused by the positional relation between the control point on the rudder and the vortex line on the wake sheet. In order to avoid infinite velocity, we introduce the Rankine vortex model to the Biot-Savart law which calculates the induced velocity by a vortex segment as shown by Equation (2) and Figure 13. The radius of the vortex core r_0 is assumed and the flow in r_0 is regarded as the rotation of a solid body.

Also, Rankine vortex model is applied to the hub vortex with validated r_0 in order to obtain the rudder drag properly.

$$\vec{v}_\gamma = \frac{1}{4\pi}\frac{\vec{r}_1\times\vec{r}_{12}}{|\vec{r}_1\times\vec{r}_{12}|^2}\left\{\frac{\vec{r}_2}{|\vec{r}_2|}-\frac{\vec{r}_1}{|\vec{r}_1|}\right\}\cdot\vec{r}_{12} \qquad (2)$$

Where

$\frac{|\vec{r}_1\times\vec{r}_{12}|}{|\vec{r}_{12}|} = d$, if $d \le r_0$ then $d = r_0$

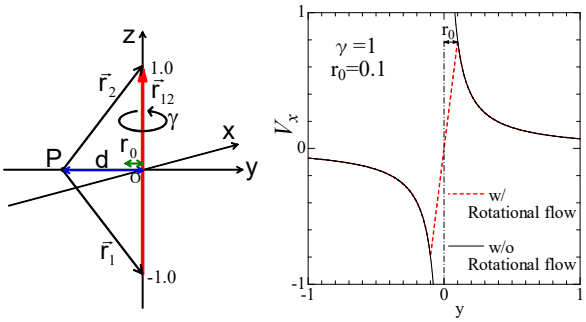

Figure 13 Induced velocity by a vortex segment

The pressure on the rudder surface p_R can be calculated by the unsteady Bernoulli Equation expressed as

$$p_R - p_0 = -\frac{1}{2}\rho(\vec{V}_r^2 - \vec{V}_{W_0}^2) - \rho\frac{\partial\phi_R}{\partial t} \qquad (3)$$

Where

p_0 : the static pressure in the undisturbed inflow

ρ : the density of the fluid

$\vec{V}_r$: the velocity vector on the rudder surface

$\vec{V}_{W_0}$: the velocity vector in the uniformed slipstream

ϕ_R: the perturbation potential on the rudder surface

$\vec{V}_{W_0}$ is calculated at a point far enough away where the acceleration gradient due to the propeller disappears, which has the same y_r, z_r as the control point on the rudder.

The pressure coefficient C_{pn} is defined using the number of revolution n and the propeller diameter D as follows:

$$C_{pn} = \frac{p_R - p_0}{\rho n^2 D^2} \qquad (4)$$

The rudder drag F_X consists of the potential flow component F_{Xpot} and the viscous drag component F_D.

$$F_X = F_{Xpot} + F_D \qquad (5)$$

Where F_{Xpot} means $F_P + F_T$ in Equation (1) and can be calculated by the pressure integration on the rudder surface as follows:

$$F_{Xpot} = \iint_{S_R}(p_R - p_0)\,n_x dS \qquad (6)$$

Where S_R and n_x are the rudder surface and the x component of the normal vector on S_R.

The calculation of F_D uses the drag coefficient formula of NACA wing section presented by Abbott & Doenhoff (1949) as follows:

$$F_D = \frac{1}{2}\rho\int_{z_s} C_{DR}(z)\vec{V}_{inx}^2(z)c(z)dz \qquad (7)$$

Where

$C_{DR} = 0.012th/c + 2(1+2th/c)C_{f(Hughes)}$

$C_{f(Hughes)} = 0.066/(log_{10}R_n - 2.03)^2$

$R_n = \frac{c(z)\vec{V}_{inx}}{\nu}$

$\tilde{V}_{inx}$ is the averaged inflow velocity in the x direction. $c(z)$ and th/c are the chord length and thickness ratio at each rudder section.

Figure 14 shows the panel arrangements for Case 1 and Case 2. The shaft cover is expressed by extending the rudder in the upward direction. It is considered that the lower end of the rudder has a mirror image effect due to the platform (Figure 6). In order to express the experimental condition in which the lower end is not the wing tip, the rudder is extended to the lower direction in the same way as the upper part. The radius of Rankine vortex core is determined to match the experimental results shown in the next chapter.

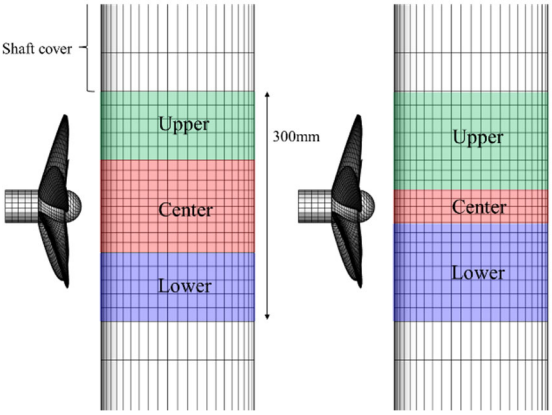

Figure 14 Panel arrangements

5 DISCUSSION

The rudder drag coefficient K_{FX} are expressed as

$$K_{FX} = \frac{F_X}{\rho n^2 D^4} \tag{8}$$

Figure 15 shows the rudder drags at the upper, center, and lower parts and the total drag obtained from the Case 1 experiment compared with each calculated result. The hub vortex core radius is set to 33% of the propeller boss radius. The calculated results agree with the experimental data both quantitatively and qualitatively, which indicates that the experimental phenomena can be expressed by appropriate modeling of the hub vortex. The experimental data at high loading condition (J=0.2) does not agree between the upper part and the lower one. This is because the wing tip flow differs between the upper end (connected to the shaft cover) and the lower end (wall by the platform) and the difference becomes remarkable at high loading condition. If we pay attention to the center part, thrust is generated at high loading condition, and it can be seen that the source of rudder thrust is located in the center part.

As well as Figure 15, Figure 16 shows the results regarding Case 2. Focusing on the drag at the center part, the slope to J becomes smaller, and even at the design point (J=0.405), the center part generates thrust. Even though the area of the center part is smaller than that of Case 1, the thrust in Case 2 is larger, which means that the thrust generated in the center part is local.

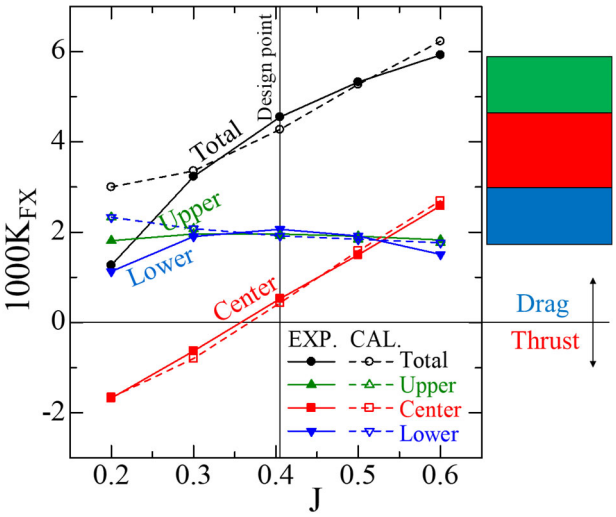

Figure 15 Rudder drags of each part (Case 1)

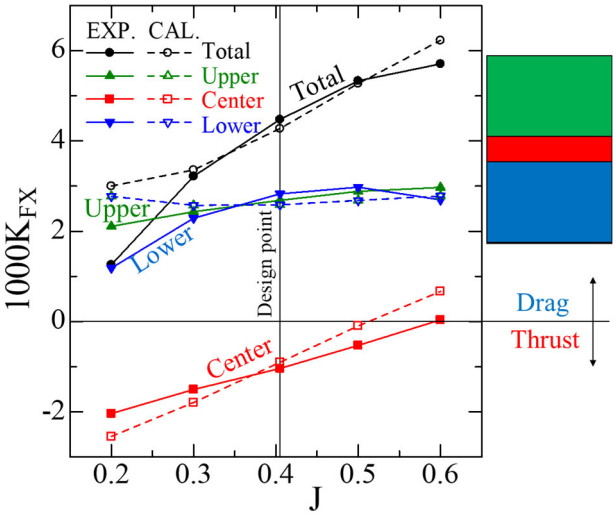

Figure 16 Rudder drags of each part (Case 2)

Figure 17 shows the calculated spanwise rudder drag distribution.

$$dK_{FX}(z) = \frac{\Delta F_X}{\rho n^2 D^4 \Delta z'} \tag{9}$$

Where

ΔF_X : the rudder drag in spanwise panel width

$\Delta z'$: the nondimensional spanwise panel width

$\Delta z' = \frac{\Delta z}{R}$

Δz : the spanwise panel width

The horizontal axis represents the sectional rudder drag coefficient by Equation (9). The vertical axis represents the position in the spanwise direction that is nondimensionalized by the propeller radius R. In this figure, the solid lines show the segmented lines for Case 2 and dotted lines show those of Case 1. Regarding Figures 15 and 16, the experimental results can be expressed by

calculation. This means that the rudder drag distribution to express these phenomena can be obtained. Also, it can be said that the increment of rudder thrust due to the high loading condition is mainly obtained at the center of the rudder.

In Figures 18 and 19, the axial velocity V_x distributions and the velocity V_y distributions obtained by calculation at the rudder leading edge line are shown dimensionless by advanced velocity V_A. V_y is equals to the circumferential velocity V_θ. In the center part of Case 2 (between solid lines), it can be seen that the acceleration in the axial velocity is small and the circumferential velocity becomes noticeably large.

As well as Figures 17, 18 and 19, Figures 20, 21 and 22 show the difference in calculated results depending on the hub vortex core radius. Though the radius affects only the center part, the thrust is very sensitive to the hub vortex core radius. How to determine the radius is our important future work.

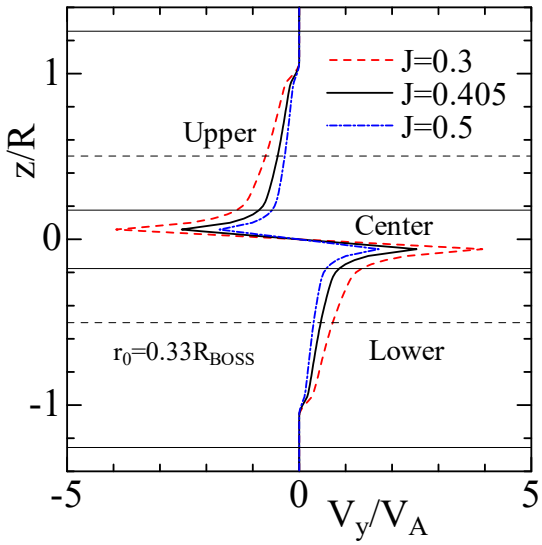

Figure 19 Calculated circumferential velocity distribution on leading edge line of rudder at each advance coefficient.

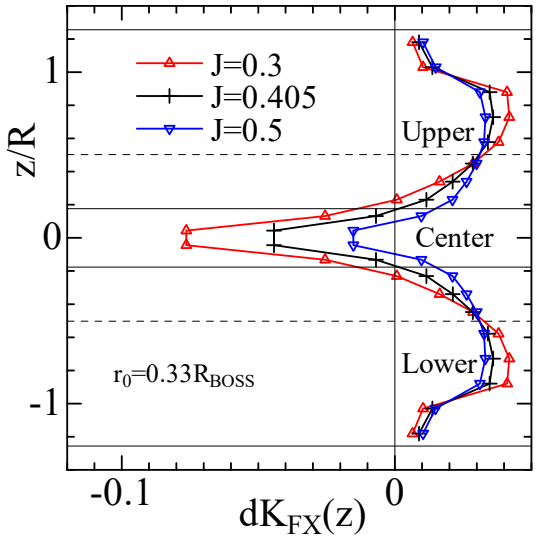

Figure 17 Calculated rudder drag distribution at each advance coefficient.

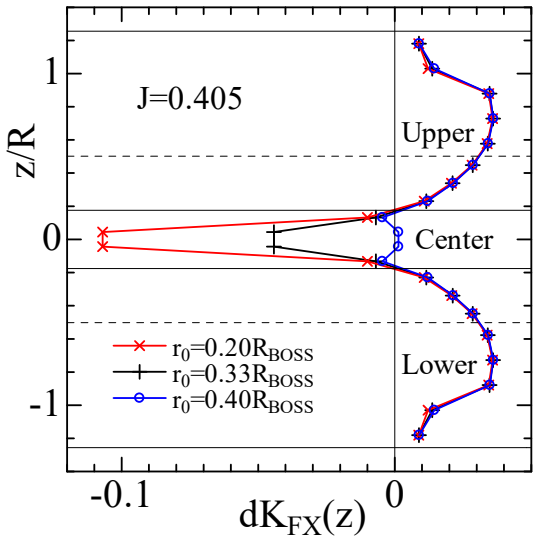

Figure 20 Calculated rudder drag distribution at each hub vortex radius.

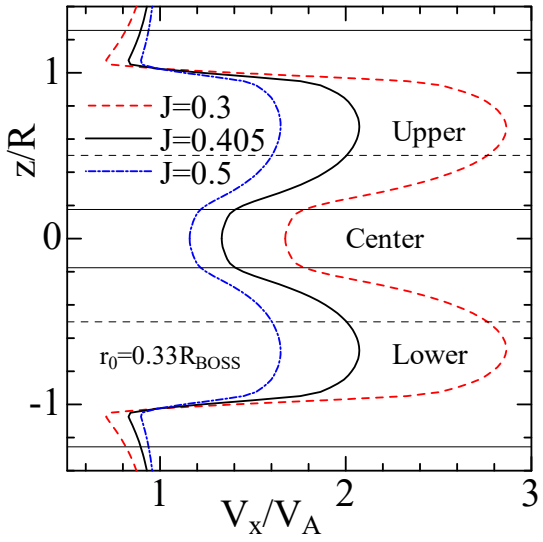

Figure 18 Calculated axial velocity distribution on leading edge line of rudder at each advance coefficient.

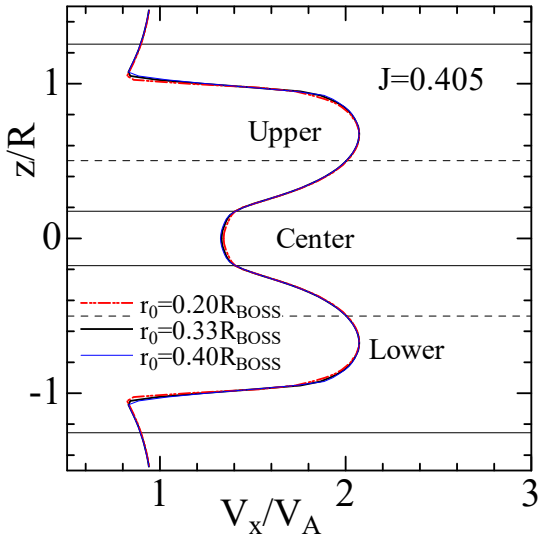

Figure 21 Calculated axial velocity distribution on leading edge line of rudder at each hub vortex radius.

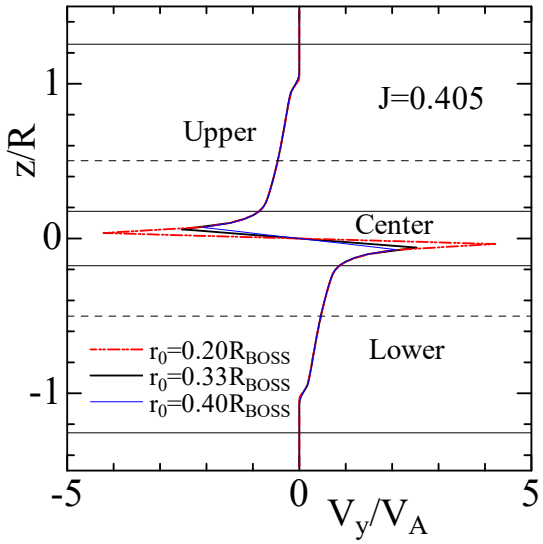

Figure 22 Calculated circumferential velocity distribution on leading edge line of rudder at each hub vortex radius.

6 CONCLUSION

In this study, in order to investigate the rudder thrust in the propeller slipstream, we conducted the rudder drag measurement using the segmented model rudder consisting of upper, center, and lower parts and obtained the rudder drag for each part. The results obtained are as follows:

1) The rudder thrust is locally generated on the center part of the rudder, which receives the hub vortex from the working propeller.
2) It is possible for the theoretical calculation by panel method to express the spanwise rudder drag distribution including the center part. On the other hand, the hub vortex core radius has a large effect on the rudder drag at the center part so how it is determined is important.

The number of experimental cases is not enough and the effect of the gaps between the segmented parts must be investigated. These are our future works.

REFERENCES

Abbott, I. H., & von Doenhoff, A. E. (1949). 'Theory of Wing Section'. McGRAW-HILL.

Ando, J., Maita, S. & Nakatake, K. (1995). 'A Simple Surface Panel Method to Predict Steady Marine Propeller Performance'. Journal of the Society of Naval Architects of Japan **178**, pp.61-69.

Hess, J. L. & Smith, A.M.O. (1964). 'Calculation of Nonlifting Potential Flow about Arbitrary Three Dimensional Bodies'. Journal of Ship Research **8**(2), pp. 22-44.

Kanemaru, T., Ryu, T., Yoshitake, A., Ando, J., & Nakatake, K. (2013). 'The Modeling of Hub Vortex for Numerical Analysis of Marine Propeller Using a Simple Surface Panel Method "SQCM" '. Proceedings of 3rd International Synposium on Marine Propulsor, Launceston, pp.365-372.

Lan, C. E. (1974). 'A Quasi-Vortex-Lattice Method in Thin Wing Theory'. Journal of Aircraft **11**(9), pp.518-527.

Maita, S., Ando, J. & Nakatake, K. (1997). 'A Simple Surface Panel Method to Predict Unsteady Marine Propeller Performance'. Journal of the Society of Naval Architects of Japan **182**, pp.71-80.

Moriyama, F. & Yamazaki, R. (1981). 'On the Effect of Propeller on Rudder'. Transactions of the West-Japan Society of Naval Architects **61**, pp.25-39.

Moriyama, F. (1981). 'On the Effect of a Rudder on Propulsive Performance'. Journal of the Society of Naval Architects of Japan **150**, pp.63-73.

Nakatake, K., Ando, J., Kataoka, K. & Yoshitake, A. (1994). 'A Simple Calculation Method for Thick Wing'. Transactions of the West-Japan Society of Naval Architects **88**, pp.13-21.

Ryu, T., Kanemaru, T., Kataoka, S., Arihama, K., Yoshitake, A., Arakawa D. & Ando, J. (2014). 'Optimization of Energy Saving Device Combined with a Propeller Using Real-Coded Genetic Algorithm'. International Journal of Naval Architecture and Ocean Engineering **6**(2), pp.406-417.